# *Impact of the North Atlantic Oscillation on transatlantic flight routes and clear-air turbulence*

# Impact of the North Atlantic Oscillation on Transatlantic Flight Routes and Clear-Air Turbulence

JUNG-HOON KIM*

*Cooperative Institute for Research in the Atmosphere, Colorado State University, Fort Collins, Colorado*

WILLIAM N. CHAN AND BANAVAR SRIDHAR

*NASA Ames Research Center, Moffett Field, California*

ROBERT D. SHARMAN

*Research Applications Laboratory, National Center for Atmospheric Research,+ Boulder, Colorado*

PAUL D. WILLIAMS

*Department of Meteorology, University of Reading, Reading, United Kingdom*

MATT STRAHAN

*NOAA/NWS/Aviation Weather Center, Kansas City, Missouri*

(Manuscript received 16 September 2015, in final form 12 January 2016)

ABSTRACT

The variation of wind-optimal transatlantic flight routes and their turbulence potential is investigated to understand how upper-level winds and large-scale flow patterns can affect the efficiency and safety of long-haul flights. In this study, the wind-optimal routes (WORs) that minimize the total flight time by considering wind variations are modeled for flights between John F. Kennedy International Airport (JFK) in New York, New York, and Heathrow Airport (LHR) in London, United Kingdom, during two distinct winter periods of abnormally high and low phases of North Atlantic Oscillation (NAO) teleconnection patterns. Eastbound WORs approximate the JFK–LHR great circle (GC) route following northerly shifted jets in the +NAO period. Those WORs deviate southward following southerly shifted jets during the −NAO period, because eastbound WORs fly closely to the prevailing westerly jets to maximize tailwinds. Westbound WORs, however, spread meridionally to avoid the jets near the GC in the +NAO period to minimize headwinds. In the −NAO period, westbound WORs are north of the GC because of the southerly shifted jets. Consequently, eastbound WORs are faster but have higher probabilities of encountering clear-air turbulence than westbound ones, because eastbound WORs are close to the jet streams, especially near the cyclonic shear side of the jets in the northern (southern) part of the GC in the +NAO (−NAO) period. This study suggests how predicted teleconnection weather patterns can be used for long-haul strategic flight planning, ultimately contributing to minimizing aviation's impact on the environment.

## 1. Introduction

Emissions from en route commercial aircraft are a significant anthropogenic contribution to global warming as air transportation over the globe grows rapidly (e.g., Lee et al. 2009, 2010). From an operational perspective, a method of reducing these emissions is to optimize flight routes in the presence of wind variations, which minimizes the total travel time and fuel consumption (e.g., Sridhar et al. 2011;

* Additional affiliation: NOAA/NWS/Aviation Weather Center, Kansas City, Missouri.

+ The National Center for Atmospheric Research is sponsored by the National Science Foundation.

*Corresponding author address*: Dr. Jung-Hoon Kim, 7220 NW 101st Terr., Kansas City, MO 64153-2317.
E-mail: jung-hoon.kim@noaa.gov; jhkim99@me.com

DOI: 10.1175/JAMC-D-15-0261.1

Kim et al. 2015). This wind-optimal route (WOR) is regarded as an efficient and environmentally friendly flight route because the amount of airborne emissions is simply a function of fuel usage, which is approximately proportional to the travel time, although other factors like $NO_x$, $O_3$, water vapor, and contrail formation need to be considered for the total climate impact (e.g., Grewe et al. 2014). These efficient WORs may not be viable if clear-air turbulence (CAT) is embedded near upper-level jets, because CAT causes safety issues and must be avoided. For commercial aircraft, CAT encounters are the leading cause of in-flight injuries among all weather-related incidents (e.g., Sharman et al. 2006). As international air traffic density increases dramatically, problems like economic costs for injuries, cabin and structural damage, and flight delays become significant. Therefore, it becomes necessary to develop routes that minimize both fuel use and the potential for CAT encounters.

Several strategies have been developed to determine WORs for air traffic management (ATM) but they do not take into account turbulence. For example, Ng et al. (2012) developed and computed WORs at multiple flight levels, which minimized total flight times by taking into account the variations of upper-level winds. Pilots' behavior during turbulence encounters and the impact on ATM has been well documented by Krozel et al. (2011), showing that CAT avoidance maneuvers depend on aircraft type and company policies. Since most of the moderate-or-greater (MOG)-level CAT encounters occur near the upper-level jet and frontal systems (e.g., Lester 1994; Wolff and Sharman 2008; Kim and Chun 2011), flight routes that approach a jet to benefit from tailwinds may incur extra fuel uses to avoid adverse turbulence encounters (e.g., Williams and Joshi 2013; Kim et al. 2015).

For long-haul transatlantic flights, WOR trajectories depend on the prevailing jet stream position and strength. Transatlantic WORs are known to be changing as the jet stream responds to climate change (Williams 2016). The CAT potential along these trajectories also depends upon weather conditions because local gradients of horizontal and vertical wind and temperature are generally large near the jet stream (e.g., Jaeger and Sprenger 2007; Williams and Joshi 2013; Karnauskas et al. 2015). The North Atlantic Oscillation (NAO) is one of the most prominent teleconnection patterns, which is composed of a north–south dipole pattern of height or pressure anomalies over the North Atlantic, especially in wintertime (e.g., Wallace and Gutzler 1981; Barnston and Livezey 1987). In the positive phase of the NAO (hereinafter referred to as +NAO), stronger pressure gradients between the persistent subtropical high and Icelandic low lead to a higher-latitude position of the jet stream.

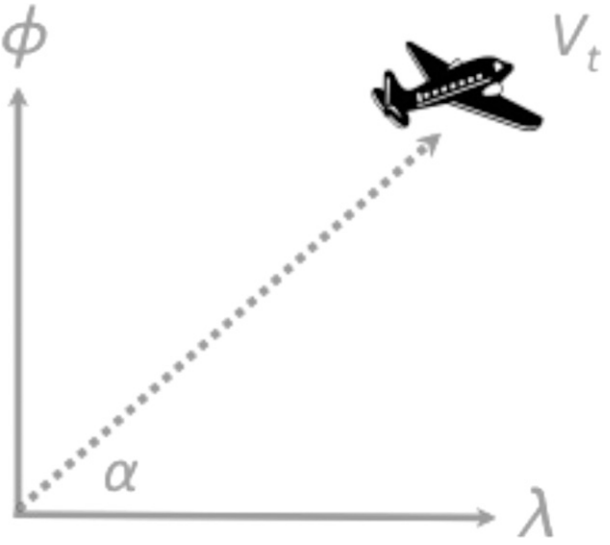


FIG. 1. Schematic of an aircraft flying horizontally over Earth's surface with a true airspeed $V_t$ and heading angle $\alpha$ during a certain period of time $\Delta t$. Here, $\phi$ and $\lambda$ are the latitudinal and longitudinal directions, respectively.

Weaker gradients in the negative phase of the NAO (hereinafter −NAO) shift the jet stream farther south, which can create different flight trajectories and environmental impacts (Irvine et al. 2013), as well as different CAT probabilities (Jaeger and Sprenger 2007). Therefore, this study aims to investigate how upper-level jet stream characteristics associated with the NAO can lead to variations in long-haul transatlantic flight routes and their CAT potential. This information can be used for efficient and safe decision-making, while also minimizing aviation's impact on the environment.

Section 2 describes the modeling of WOR trajectories, and section 3 examines deviations of the transatlantic WORs and their CAT potential during two winter seasons with distinct NAO patterns. The summary and conclusions are discussed in section 4.

## 2. Modeling of WOR aircraft trajectories

When an aircraft is flying horizontally above Earth's surface with a true airspeed $V_t$ and heading angle $\alpha$ during a certain period of time $\Delta t$, as shown in Fig. 1, the longitudinal $\lambda$ and latitudinal $\phi$ position changes of the aircraft with time in the presence of horizontal winds are governed by the following aircraft-motion equations (e.g., Sridhar et al. 2011; Ng et al. 2012; Kim et al. 2015):

$$\frac{d\lambda(t)}{dt} = \frac{V_t \cos\alpha(t) + u(\lambda, \phi, z)}{R\cos\phi(t)} \quad \text{and} \tag{1}$$

$$\frac{d\phi(t)}{dt} = \frac{V_t \sin\alpha(t) + v(\lambda, \phi, z)}{R}. \tag{2}$$

Here, $R$ is Earth's radius (Earth is assumed to be a sphere); $z \ll R$ is the height above the surface; and $u$ and $v$ are the zonal and meridional wind components, respectively. The value of $V_t$ is a constant of 250 m s$^{-1}$ (which is representative of the general airspeed of commercial flight).

To maximize the advantage of a tailwind and/or minimize the disadvantage of a headwind in the modeling of an aircraft trajectory, we need to take into account wind variations in the calculation of the heading angle $\alpha$ at each time step to minimize the total travel time from departure to destination. To compute the WOR, the aircraft $\alpha$ is regarded as a control parameter. Then, the analytic solution of $\alpha$ that minimizes the total cost function (i.e., total travel time) is derived by Pontryagin's minimum principle (Bryson and Ho 1975):

$$J = \int_{t_0}^{t_f} C_t \, dt. \tag{3}$$

Here, $C_t$ is the cost coefficient of travel time ($C_t = 1$ in this study), and $t_0$ and $t_f$ are the times at the departure and arrival airports, respectively. The analytic solution for the control parameter of $\alpha$ that takes into account the variations of the winds in Eqs. (1) and (2) and minimizes the total cost function in Eq. (3) is

$$\frac{d\alpha(t)}{dt} = -\frac{F_{\text{wind}}(t)}{C_t R \cos\phi(t)}, \quad \text{where}$$

$$\begin{aligned} F_{\text{wind}}(t) = &-\sin\alpha(t)\cos\alpha(t)\frac{\partial u(\lambda,\phi,z)}{\partial\lambda} + \cos^2\alpha(t)\sin\phi(t)u(\lambda,\phi,z) + \cos^2\alpha(t)\cos\phi(t)\frac{\partial u(\lambda,\phi,z)}{\partial\phi} \\ &- \frac{\partial v(\lambda,\phi,z)}{\partial\lambda} + \sin\alpha(t)\cos\alpha(t)\sin\phi(t)v(\lambda,\phi,z) + \cos\alpha(t)\sin\alpha(t)\cos\phi(t)\frac{\partial v(\lambda,\phi,z)}{\partial\phi} \\ &+ V_t\cos\alpha(t)\sin\phi(t) + \cos^2\alpha(t)\frac{\partial v(\lambda,\phi,z)}{\partial\lambda}. \end{aligned} \tag{4}$$

A full derivation of the analytic solution in Eq. (4) can be found in previous studies (e.g., Sridhar et al. 2011; Ng et al. 2012; Kim et al. 2015). In the next stage, the optimal initial heading angle $\alpha(t_0)$ at the departure airport is determined as follows. First, the great circle (GC) heading angle $\alpha_{\text{GC}}$ between the departure and arrival airports is selected as a first guess for the optimal heading angle (Kim et al. 2015). Then, Eqs. (1), (2), and (4) are solved using the explicit Euler forward integration scheme $\{y(t+1) = y(t) + \Delta t[dy(t)/dt]$, where $y = \lambda, \phi,$ and $\alpha\}$ from the departure to the destination. This process is iterated with different $\alpha(t_0)$ ranging between $\alpha_{\text{GC}} - 45°$ and $\alpha_{\text{GC}} + 45°$ with an increment of 2.5° until each trajectory meets the termination condition of either 1) the minimum distance between the trajectory and the final destination is smaller than 100 km or 2) the distance between each trajectory and the initial departure airport is greater than 1.2 times the total GC distance between the departure and arrival destinations. Finally, among these, the trajectory that arrives at the destination faster than any of the others is chosen as the WOR. Because $V_t$ is fixed in Eqs. (1) and (2) in this study, the calculated WOR is time optimal at a given flight level.

Figure 2 shows an example of the WOR calculations for eastbound (EB) and westbound (WB) routes at 250 hPa (about $z = 11$ km) between John F. Kennedy International Airport (JFK) in New York, New York, and Heathrow Airport (LHR) in London, United Kingdom, for 0000 and 1200 UTC 3 January 2005 (left and right panels, respectively). In this example, wind data are from the 6-hourly Modern-Era Retrospective Analysis for Research and Applications (MERRA) reanalysis data with ½° (latitude) × ⅔° (longitude) horizontal grid spacing. The time step $\Delta t = 180$ s (3 min) for the trajectory modeling by Eqs. (1), (2), and (4) with $V_t$ of 250 m s$^{-1}$, which roughly corresponds to the resolution of the MERRA wind data. EB (gray lines in Fig. 2, top left) and WB (gray lines in Fig. 2, top right) trajectories reach different regions according to the initial heading angles selected in a given wind situation, which corresponds to the minimum distance between each trajectory and the destination in Fig. 2 (bottom). The fastest one to the destination has been picked up as the EB WOR (thick blue line in Fig. 2, top left) and WB WOR (thick red line in Fig. 2, top right) in this wind condition. For a reference, the GC route between JFK and LHR is depicted by the thick black line.

The total flight time along this GC with still air (no wind) would be 368 min with $V_t$ of 250 m s$^{-1}$. In this case, the EB WOR (blue line) follows the strong westerly and southwesterly jet over the North Atlantic to maximize

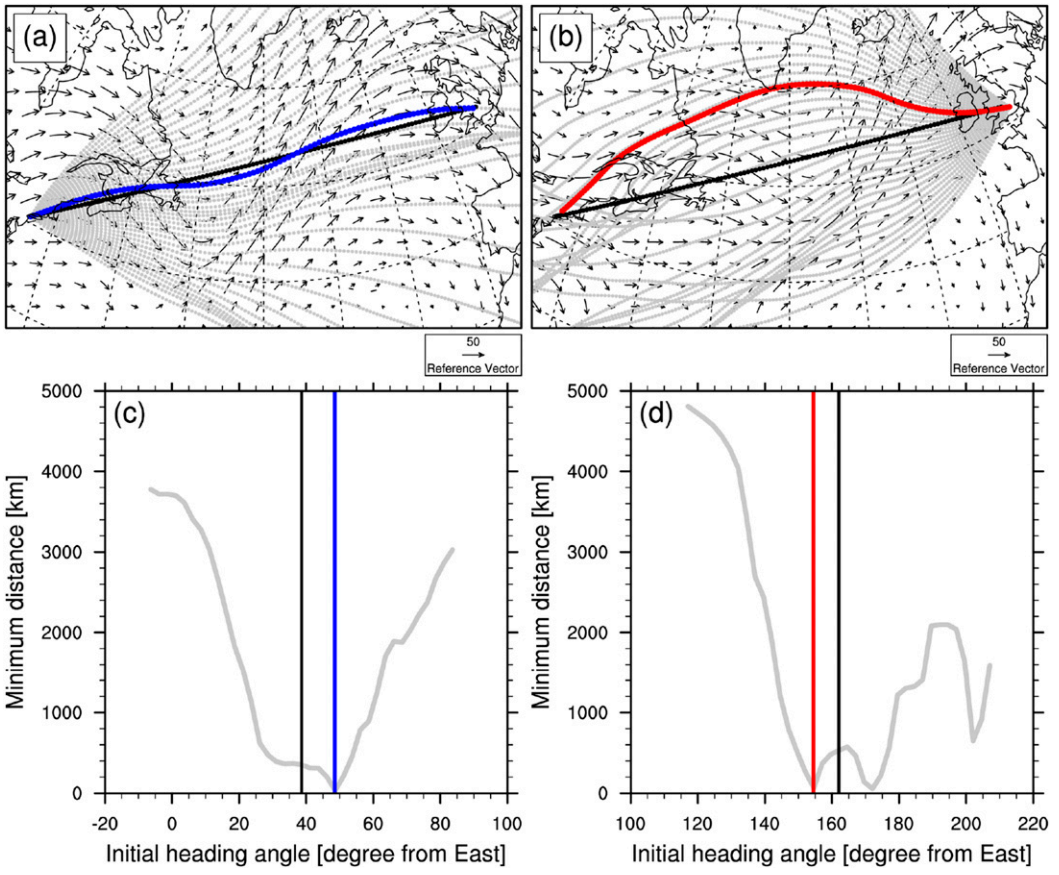


FIG. 2. (a) EB (thick blue) and (b) WB (thick red) WORs between JFK and LHR with candidate trajectories (gray lines) from different initial heading angles ranging from GC heading angle $\alpha_{GC} - 45°$ to $\alpha_{GC} + 45°$ with 2.5° bins and horizontal winds vectors at (left) 0000 and (right) 1200 UTC 3 Jan 2005 at 250 hPa (about $z = 11$ km or 34 000 ft). Corresponding minimum distances (km) between the trajectories and the destination airport for (c) EB and (d) WB. Reference wind vectors to the bottom right of (a) and (b) are 50 m s$^{-1}$. The optimal EB (blue) and WB (red) flight routes having the minimum time and distance are shown in the left and right plots. In all plots, the black line is the GC route between JFK and LHR.

its tailwind (Fig. 2a; 321 min of total flight time). The WB WOR (red line) detours northward near the southern tip of Greenland to avoid the prevailing westerly jet flow, thereby minimizing its headwind (Fig. 2b; 417 min of total flight time). It is noted that in Figs. 2b and 2d the WB trajectory with the initial heading angle of the GC routes (162°) does not go directly to JFK and has a longer flight time than two other WB trajectories as it avoids the jet stream. In this case, the northerly route with $\alpha(t_0) = 154.5°$ (red line) is selected as the WB WOR because this is 1 min faster than the southerly detouring route with $\alpha(t_0) = 172°$ to the JFK in a given wind condition.

## 3. Results

Variations of the WORs and their CAT potential between the JFK and LHR are investigated during two distinct winter seasons [December 2004–February 2005 (DJF04–05) and December 2009–February 2010 (DJF09–10)]. The two seasons are selected because monthly averaged values of the NAO index during DJF04–05 are highly positive (+1.21 in December and +1.52 in January), while they are extremely negative during DJF09–10 (−1.92 in December and −1.11 in January) according to the Climate Prediction Center. These periods were already selected for the study of aviation's impact on the environment based on weather patterns in Irvine et al. (2013).

Figure 3 shows the averaged horizontal wind speed (Figs. 3a,b), as well as the variability of the EB (blue lines; Figs. 3c,d) and WB (red lines; Figs. 3e,f) WORs at 250 hPa during DJF 04–05 (Figs. 3a,c,e) and DJF 09–10 (Figs. 3b,d,f). In this study, the EB (WB) WORs are launched at 0000 (1200) UTC each day during the study

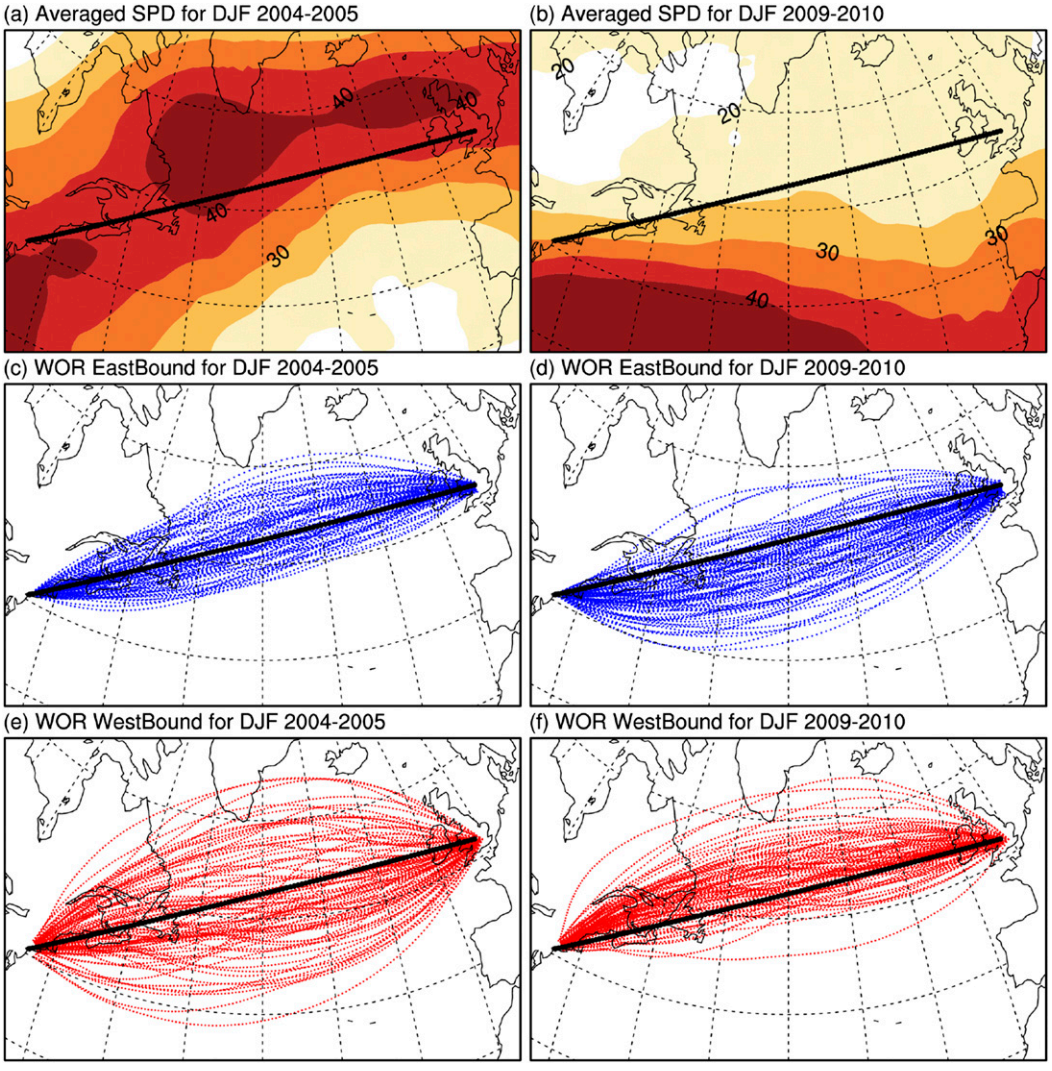


FIG. 3. (top) Averaged horizontal wind speed (shadings from 10 to 50 m s$^{-1}$ with 10 m s$^{-1}$ interval) and variations of the WORs at 250 hPa between JFK and LHR for (middle) EB (blue-dotted lines) and (bottom) WB (red-dotted lines) during (a),(c),(e) DJF04–05 and (b),(d),(f) DJF09. The GC between JFK and LHR is depicted as a reference (black line) in all plots.

periods, which corresponds to a maximum of actual air traffic in the North Atlantic corridor (Schumann and Graf 2013), and the route between JFK and LHR is selected as a representative transatlantic flight route (Irvine et al. 2013). Figures 3a and 3b show distinct jet streams in two different NAO phases. Because of the interannual variability of persistent high and low pressure systems in the North Atlantic, the dominant jet stream shifts northward directly to northwestern Europe in +NAO (Fig. 3a) and moves southward closer to southern Europe in −NAO, which is consistent with results from previous studies (e.g., Barnston and Livezey 1987; Jaeger and Sprenger 2007; Irvine et al. 2013).

In Figs. 3c–f, the overall features of the EB (blue lines in Figs. 3c and 3d) and WB (red lines in Figs. 3e and 3f) WORs are different between the two designated winter seasons. The EB WORs from JFK to LHR usually follow the prevailing westerly jet stream to maximize tailwinds, thereby reducing total travel time and fuel consumption. In particular, the EB WORs are close to the GC between JFK and LHR (a black reference line) and distributed both north and south directly to northern Europe following northerly shifted jets in the +NAO phase during DJF04–05 (Fig. 3c). EB WORs are more southerly toward southern Europe and the Mediterranean Sea (Fig. 3d), following the southerly shifted jet streams in the −NAO phase during DJF09–10

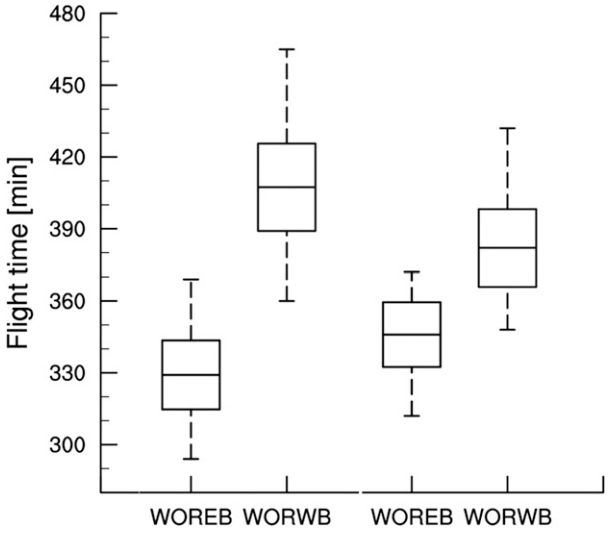


FIG. 4. Bar charts of the mean, mean ± 2 standard deviations, and minimum and maximum values of the travel times along the EB and WB WORs between JFK and LHR shown in Fig. 3 during the +NAO phase during DJF04–05 (left two boxes) and −NAO phase during DJF09–10 (right two boxes).

(Fig. 3b). These results are consistent with the flight trajectories in weather pattern 2 in Irvine et al. (2013; see their Fig. 7). The WB WORs from LHR to JFK, however, avoid the prevailing westerly jet stream to minimize their headwinds. In the +NAO phase during DJF04–05 (Fig. 3e), the WB WORs deviate southward or northward to avoid the strong jet stream dominating along the GC, so that the envelope of the WB WORs becomes meridionally spread. However, in the −NAO phase during DJF09–10 (Fig. 3f), as a result of the southerly shifted westerly jet stream, the WB WORs are mostly around the northern part of the GC (Fig. 3f). This is similar to the trajectories of weather pattern 4 in Irvine et al. (2013; see their Fig. 7).

Figure 4 shows bar charts of the mean, ± 2 standard deviations, and maximum and minimum values of the flight times for the EB and WB WORs during the +NAO (DJF04–05; leftmost two) and −NAO (DJF09–10; rightmost two). First, EB WORs are faster than WB WORs, as expected from Fig. 3. Second, the difference in total travel time between EB and WB WORs is greater in the +NAO phase during DJF04–05 than in the −NAO phase during DJF09–10, because the prevailing westerly jet along the GC is stronger in +NAO than −NAO phases as shown in Figs. 3a and 3b. Third, EB WORs (WB WORs) in +NAO (−NAO) phase are faster than those in −NAO (+NAO), because the distances of the EB WORs (WB WORs) are smaller in +NAO (−NAO) phase as well as tailwinds (headwinds) that are stronger in +NAO (−NAO) phase (Figs. 3c–f).

Based on the aforementioned variability of the WORs in each period, the differences in CAT potential along these WORs can be investigated using the MERRA data with 50-hPa vertical grid spacing between the 400- and 100-hPa levels, because grid-resolvable strong vertical wind shears and temperature gradients can be a good indicator for aircraft-scale turbulence (e.g., Sharman et al. 2006; Jaeger and Sprenger 2007; Kim et al. 2011; Williams and Joshi 2013). Figures 5a and 5b show the averaged values of the turbulence index 1 (TI1) for two winter periods. The TI1 diagnostic is a combination of vertical shear and total deformation, which is a simplified version of upper-level frontogenesis that is a typical CAT generation mechanism, especially above and below the jet core on the cyclonic shear side of the jet streak (Ellrod and Knapp 1992). Thus, it is most skillful and is the most widely used CAT indicator in operational forecasts (e.g., Sharman et al. 2006; Kim et al. 2011; Gill 2014):

$$\mathrm{TI1}(x,y,z) = \mathrm{VWS}(x,y,z) \times \mathrm{DEF}(x,y,z), \quad \text{where}$$

$$\mathrm{VWS}(x,y,z) = \left\{ \left[\frac{\partial u(x,y,z)}{\partial z}\right]^2 + \left[\frac{\partial v(x,y,z)}{\partial z}\right]^2 \right\}^{1/2} \quad \text{and}$$

$$\mathrm{DEF}(x,y,z) = \left[\frac{\partial v(x,y,z)}{\partial x} + \frac{\partial u(x,y,z)}{\partial y}\right]^2 + \left[\frac{\partial u(x,y,z)}{\partial x} - \frac{\partial v(x,y,z)}{\partial y}\right]^{1/2}.$$

In Figs. 5a and 5b, higher values of the averaged TI1 in northern parts of the JFK–LHR GC in +NAO and southern parts in −NAO correspond to the cyclonic shear side of the jets shown in Figs. 3a and 3b, which is more obvious in Fig. 5c for the difference in the averaged TI1 between two periods. Considering the variations of EB and WB WORs shown in Figs. 3c–f, the EB WORs would pass more frequently through higher TI1 areas during both winter periods. As an example, Fig. 5d shows a snapshot for the TI1 with horizontal wind vectors at 250 hPa during 3 January 2005. During this time, the WB WOR (red line) passed through less area with higher CAT potential, because it deviates northward to avoid the prevailing westerly and southwesterly flows (it might be also small when it would detour southward), while EB WOR (blue line) encountered higher CAT potential areas for a longer period of time.

The probability density functions (PDFs) for TI1 along the EB and WB WORs during two winter seasons are investigated. Figure 6 shows PDFs for TI1 along the EB (blue) and WB (red) WORs in +NAO (DJF04–05).

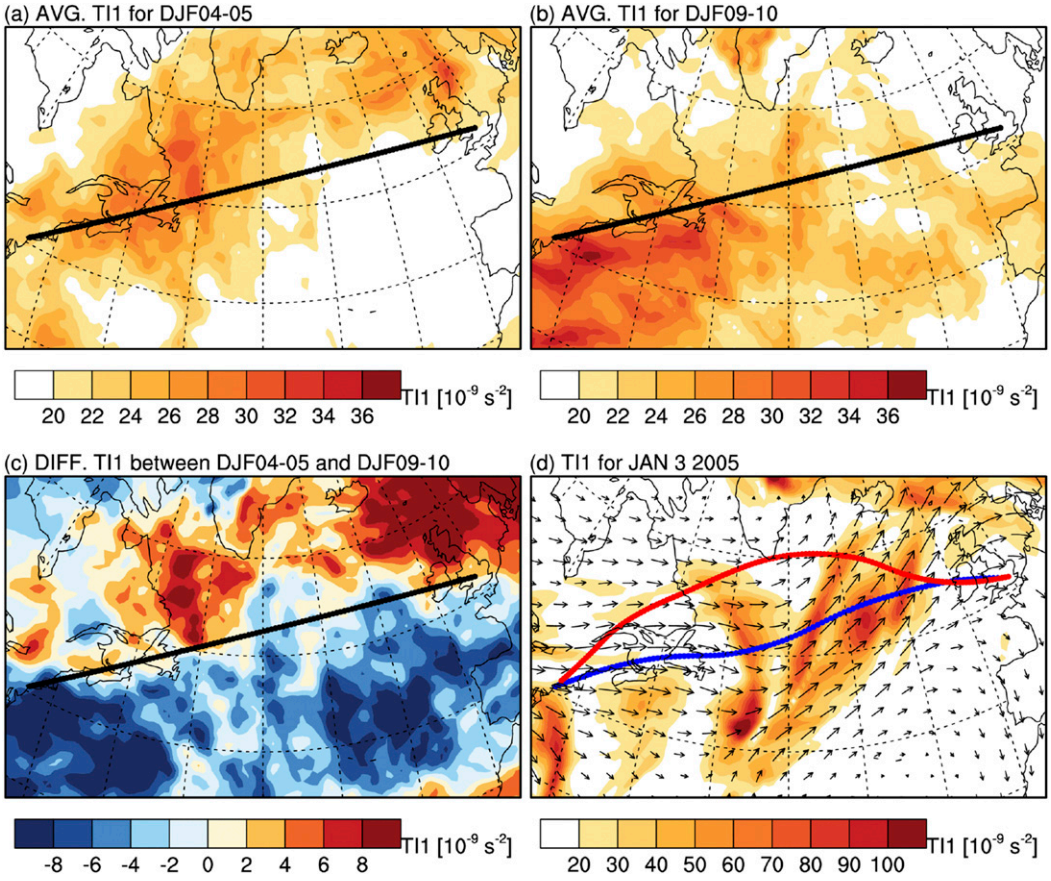


FIG. 5. Shadings of averaged TI1 ($s^{-2}$) for (a) +NAO phase during DJF04–05 and (b) −NAO phase in DJF09–10, and (c) their difference. (d) EB (blue) and WB (red) WORs with TI1 (shading) and horizontal wind vectors at the 250-hPa level between JFK and LHR on 3 Jan 2005. Note that the shading levels for the TI1 in the top and bottom panels are different.

Overlaps between EB and WB WORs are depicted as orange color bars. The median of EB WORs (blue; $23.4 \times 10^{-9}\,s^{-2}$) is higher than that of WB WORs (red; $21.5 \times 10^{-9}\,s^{-2}$). Median values of the PDFs for EB and WB WORs during two winter periods are summarized in Table 1. The probability of the 99th percentile value ($13.4 \times 10^{-8}\,s^{-2}$) of TI1, approximately representing MOG-level CAT, has also been calculated and tabulated in Table 1. As expected, the medians of CAT for EB WORs are higher than those of WB WORs during both winter periods. The chances of encountering MOG-level CAT are also higher along the EB WORs than the WB WORs because they are following the jet stream where CAT potential is higher. Especially, EB WORs in −NAO have the highest chance because most trajectories tend to pass directly to the cyclonic shear side of the southerly shifted jet stream (e.g., Figs. 3d and 5b). For the WB WORs, the +NAO phase has a higher median value and higher chances for MOG-level CAT because some of the WB WORs detouring northward would encounter high CAT potential areas on the cyclonic shear side of the northerly shifted jet stream in +NAO (e.g., Figs. 3e and 5a). For the confidence test, 200 half-portions of the total TI1 data sample along the WORs have been randomly selected to make the same PDFs, medians, and the MOG-level CAT probabilities in Table 1. Among the 200, the maximum and minimum values of medians and MOG-level CAT probabilities are within ±10% of the values in Table 1, which shows that the results in Table 1 are statistically significant (e.g., Sharman et al. 2006; Kim et al. 2011).

## 4. Summary and conclusions

In this study, the variations of transatlantic WORs between JFK and LHR, and their CAT potential, during two different winter seasons were investigated. Simplified aircraft trajectory models were derived by applying the minimal principal theory to the control parameter of aircraft heading angle in the presence of winds. Results

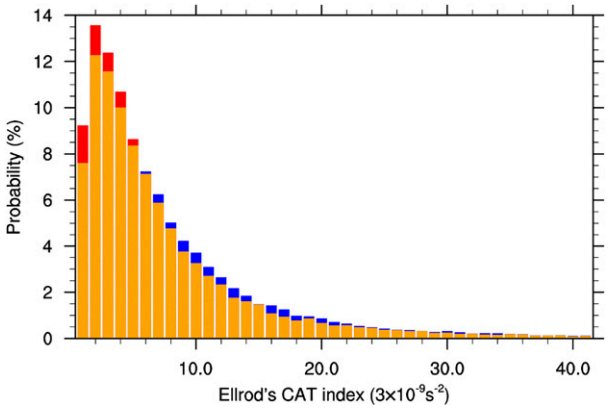


FIG. 6. PDFs for TI1 ($s^{-2}$) along the EB (blue bars) and WB (red bars) WORs during +NAO phase during DJF04–05. Overlaps of the PDFs between EB and WB WORs are shown by orange bars.

show the variability of WORs and their CAT potential during two distinct upper-level flow patterns. Depending on the upper-level winds, the modeled WORs had different flight trajectories and flight times (and, consequently, fuel burned). EB WORs are close to the GC between JFK and LHR by following northerly shifted jet streams in +NAO, while EB WORs deviate southward by taking advantage of the southerly shifted jets in −NAO. WB WORs, however, detoured northward or southward of the prevailing jets along the GC, which spreads out the trajectories meriodionally in +NAO, but those are along the GC in −NAO because of the southerly shifted jets. Eventually, EB WORs were faster than WB WORs. EB WORs in +NAO are faster than those in −NAO, because the jet stream along the GC is stronger in +NAO. EB WORs had a higher probability of encountering MOG-level CAT than WB WORs, as they pass through the higher regions of vertical and horizontal wind shears near the jet stream in both winter periods. In particular, the EB WOR trajectories in the −NAO period are in phase with high CAT potential in the cyclonic shear side of the southerly shifted jets.

This information can be used in the aviation sector to understand how the predicted upper-level teleconnection weather patterns can be translated to make a decision for safe and efficient long-haul transatlantic flight routes. For example, the predicted jet stream would be shifted northward in a +NAO pattern, so a pilot from JFK to LHR (i.e., EB) could fly on the anticyclonic shear side of the jet streak and a pilot from LHR to JFK (i.e., WB) could detour southward rather than northward of the jet streak. This routing eventually yields social benefits by producing efficient and safe flights and also reduces the impacts on the environment, although more impacts from $NO_x$-induced $O_3$ and water vapor in the stratosphere, contrail formations in ice supersaturated regions, and noise near airports should be also considered for climate-optimal and environmentally sound WORs (e.g., Köhler et at. 2008; Grewe and Stenke 2008; Grewe et al. 2014). WORs and their adverse CAT encounters can be changed by upper-level weather patterns, which can be also applied to future climate scenarios (e.g., Williams and Joshi 2013). Further studies designed to investigate other types of CAT indicators related to spontaneous imbalance (e.g., Knox et al. 2008), mountain waves (e.g., Kim and Chun 2010; Sharman et al. 2012), and deep convection (e.g., Kim and Chun 2012; Kim et al. 2014; Trier and Sharman 2009), or a combined indicator like graphical turbulence guidance (GTG; Sharman et al. 2006; Kim et al. 2011; Gill 2014), should be priorities for future research. Other types of weather constraints such as deep convection, icing, volcanic ash, as well as climate concerns like $NO_2$ and water vapor emissions in stratosphere and contrail formations (e.g., Grewe and Stenke 2008; Grewe et al. 2014), can be also considered in optimizing routes using similar techniques in the future.

TABLE 1. Median values of TI1 ($s^{-2}$) and probability for MOG-level turbulence along the EB and WB WORs during +NAO and −NAO during DJF04–05 and DJF09–10, respectively.

| | DJF 04–05 (+NAO) | | DJF 09–10 (−NAO) | |
|---|---|---|---|---|
| | Median ($s^{-2}$) | MOG (%) | Median ($s^{-2}$) | MOG (%) |
| EB | $2.34 \times 10^{-8}$ | 1.02 | $2.59 \times 10^{-8}$ | 1.31 |
| WB | $2.15 \times 10^{-8}$ | 0.92 | $2.29 \times 10^{-8}$ | 0.81 |

*Acknowledgments.* This research is in response to requirements and funding by the U.S. Federal Aviation Administration (FAA). The views expressed are those of the authors and do not necessarily represent the official policy and position of the FAA. The authors thank three anonymous reviewers for their invaluable comments and suggestions.

## REFERENCES

Barnston, A. G., and R. E. Livezey, 1987: Classification, seasonality and persistence of low-frequency atmospheric circulation patterns. *Mon. Wea. Rev.*, **115**, 1083–1126, doi:10.1175/1520-0493(1987)115<1083:CSAPOL>2.0.CO;2.

Bryson, A. E., and Y. C. Ho, 1975: *Applied Optimal Control.* Taylor and Francis, 481 pp.

Ellrod, G. P., and D. I. Knapp, 1992: An objective clear-air turbulence forecasting technique: Verification and operational use. *Wea. Forecasting*, **7**, 150–165, doi:10.1175/1520-0434(1992)007<0150:AOCATF>2.0.CO;2.

Gill, P. G., 2014: Objective verification of World Area Forecast Centre clear air turbulence forecasts. *Meteor. Appl.*, **21**, 3–11, doi:10.1002/met.1288.

Grewe, V., and A. Stenke, 2008: AirClim: An efficient tool for climate evaluation of aircraft technology. *Atmos. Chem. Phys.*, **8**, 4621–4639, doi:10.5194/acp-8-4621-2008.

——, T. Champougny, S. Matthes, C. Frömming, S. Brinkop, O. A. Søvde, E. A. Irvine, and L. Halscheidt, 2014: Reduction of the air traffic's contribution to climate change: A REACT4C case study. *Atmos. Environ.*, **94**, 616–625, doi:10.1016/j.atmosenv.2014.05.059.

Irvine, E. A., B. J. Hoskins, K. P. Shine, R. W. Lunnon, and C. Froemming, 2013: Characterizing North Atlantic weather patterns for climate-optimal aircraft routing. *Meteor. Appl.*, **20**, 80–93, doi:10.1002/met.1291.

Jaeger, E. B., and M. Sprenger, 2007: A Northern Hemispheric climatology of indices for clear air turbulence in the tropopause region derived from ERA40 reanalysis data. *J. Geophys. Res.*, **112**, D20106, doi:10.1029/2006JD008189.

Karnauskas, K. B., J. P. Donnelly, H. C. Barkley, and J. E. Martin, 2015: Coupling between air travel and climate. *Nat. Climate Change*, **5**, 1068–1073, doi:10.1038/nclimate2715.

Kim, J.-H., and H.-Y. Chun, 2010: A numerical study of clear-air turbulence (CAT) encounters over South Korea on 2 April 2007. *J. Appl. Meteor. Climatol.*, **49**, 2381–2403, doi:10.1175/2010JAMC2449.1.

——, and ——, 2011: Statistics and possible sources of aviation turbulence over South Korea. *J. Appl. Meteor. Climatol.*, **50**, 311–324, doi:10.1175/2010JAMC2492.1.

——, and ——, 2012: A numerical simulation of convectively induced turbulence above deep convection. *J. Appl. Meteor. Climatol.*, **51**, 1180–1200, doi:10.1175/JAMC-D-11-0140.1.

——, ——, R. D. Sharman, and T. L. Keller, 2011: Evaluations of upper-level turbulence diagnostics performance using the Graphical Turbulence Guidance (GTG) system and pilot reports (PIREPs) over East Asia. *J. Appl. Meteor. Climatol.*, **50**, 1936–1951, doi:10.1175/JAMC-D-10-05017.1.

——, ——, ——, and S. B. Trier, 2014: The role of vertical shear on aviation turbulence within cirrus bands of a simulated western Pacific Ocean. *Mon. Wea. Rev.*, **142**, 2794–2813, doi:10.1175/MWR-D-14-00008.1.

——, W. N. Chan, B. Sridhar, and R. D. Sharman, 2015: Combined winds and turbulence prediction system for automated air-traffic management applications. *J. Appl. Meteor. Climatol.*, **54**, 766–784, doi:10.1175/JAMC-D-14-0216.1.

Knox, J. A., D. W. McCann, and P. D. Williams, 2008: Application of the Lighthill–Ford theory of spontaneous imbalance to clear-air turbulence forecasting. *J. Atmos. Sci.*, **65**, 3292–3304, doi:10.1175/2008JAS2477.1.

Köhler, M. O., G. Rädel, O. Dessens, K. P. Shine, H. L. Rogers, O. Wild, and J. A. Pyle, 2008: Impact of perturbations to nitrogen oxide emissions from global aviation. *J. Geophys. Res.*, **113**, D11305, doi:10.1029/2007JD009140.

Krozel, J., V. Klimenko, and R. D. Sharman, 2011: Analysis of clear-air turbulence avoidance maneuvers. *Air Traffic Control Quart.*, **4**, 147–168.

Lee, D. S., D. W. Fahey, P. M. Forster, P. J. Newton, R. C. N. Wit, L. L. Lim, B. Owen, and R. Sausen, 2009: Aviation and global climate change in the 21st century. *Atmos. Environ.*, **43**, 3520–3537, doi:10.1016/j.atmosenv.2009.04.024.

——, and Coauthors, 2010: Transport impacts on atmosphere and climate: Aviation. *Atmos. Environ.*, **44**, 4678–4734, doi:10.1016/j.atmosenv.2009.06.005.

Lester, P. F., 1994: *Turbulence: A New Perspective for Pilots*. Jeppesen Sanderson, 212 pp.

Ng, H. K., B. Sridhar, and S. Grabbe, 2012: A practical approach for optimizing aircraft trajectories in winds. *31st Digital Avionics Systems Conf.*, Williamsburg, VA, IEEE, 3D6-1–3D6-14. [Available online at http://www.aviationsystemsdivision.arc.nasa.gov/publications/2012/DASC2012_Ng.pdf.]

Schumann, U., and K. Graf, 2013: Aviation-induced cirrus and radiation changes at diurnal timescales. *J. Geophys. Res. Atmos.*, **118**, 2404–2421, doi:10.1002/jgrd.50184.

Sharman, R. D., C. Tebaldi, G. Wiener, and J. Wolff, 2006: An integrated approach to mid- and upper-level turbulence forecasting. *Wea. Forecasting*, **21**, 268–287, doi:10.1175/WAF924.1.

——, J. D. Doyle, and M. A. Shapiro, 2012: An investigation of a commercial aircraft encounter with severe clear-air turbulence over western Greenland. *J. Appl. Meteor. Climatol.*, **51**, 42–53, doi:10.1175/JAMC-D-11-044.1.

Sridhar, B., H. K. Ng, and N. Y. Chen, 2011: Aircraft trajectory optimization and contrails avoidance in the presence of winds. *J. Guidance, Control, Dyn.*, **34**, 1577–1584, doi:10.2514/1.53378.

Trier, S. B., and R. D. Sharman, 2009: Convection-permitting simulations of the environment supporting widespread turbulence within the upper-level outflow of a mesoscale convective system. *Mon. Wea. Rev.*, **137**, 1972–1990, doi:10.1175/2008MWR2770.1.

Wallace, J. M., and D. S. Gutzler, 1981: Teleconnections in the geopotential height field during the Northern Hemisphere winter. *Mon. Wea. Rev.*, **109**, 784–812, doi:10.1175/1520-0493(1981)109<0784:TITGHF>2.0.CO;2.

Williams, P. D., 2016: Transatlantic flight times and climate change. *Environ. Res. Lett.*, **11**, 024008, doi:10.1088/1748-9326/11/2/024008.

——, and M. M. Joshi, 2013: Intensification of winter transatlantic aviation turbulence in response to climate change. *Nat. Climate Change*, **3**, 644–648, doi:10.1038/nclimate1866.

Wolff, J. K., and R. D. Sharman, 2008: Climatology of upper-level turbulence over the contiguous United States. *J. Appl. Meteor. Climatol.*, **47**, 2198–2214, doi:10.1175/2008JAMC1799.1.